Shear stress influences spatial variations in vascular Mn-SOD expression: implication for LDL nitration

Lisong Ai,[1]* Mahsa Rouhanizadeh,[1]* Joseph C. Wu,[2] Wakako Takabe,[1] Hongyu Yu,[1] Mohammad Alavi,[3] Rongsong Li,[1] Yi Chu,[4] Jordan Miller,[4] Donald D. Heistad,[4] and Tzung K. Hsiai[1]

[1]*Department of Biomedical Engineering and Cardiovascular Medicine, University of Southern California, Los Angeles, California;* [2]*Department of Medicine, Division of Cardiology, Stanford University School of Medicine, Stanford, California;* [3]*Department of Pathology, University of Southern California, Los Angeles, California; and* [4]*Department of Internal Medicine, University of Iowa Carver College of Medicine and VA Medical Center, Iowa City, Iowa*

Submitted 4 November 2007; accepted in final form 11 April 2008

Ai L, Rouhanizadeh M, Wu JC, Takabe W, Yu H, Alavi M, Li R, Chu Y, Miller J, Heistad DD, Hsiai TK. Shear stress influences spatial variations in vascular Mn-SOD expression: implication for LDL nitration. *Am J Physiol Cell Physiol* 294: C1576–C1585, 2008. First published April 23, 2008; doi:10.1152/ajpcell.00518.2007.— Fluid shear stress modulates vascular production of endothelial superoxide anion ($O_2^{\cdot-}$) and nitric oxide ($^{\cdot}NO$). Whether the characteristics of shear stress influence the spatial variations in mitochondrial manganese superoxide dismutase (Mn-SOD) expression in vasculatures is not well defined. We constructed a three-dimensional computational fluid dynamics model simulating spatial variations in shear stress at the arterial bifurcation. In parallel, explants of arterial bifurcations were sectioned from the human left main coronary bifurcation and right coronary arteries for immunohistolocalization of Mn-SOD expression. We demonstrated that Mn-SOD staining was prominent in the pulsatile shear stress (PSS)-exposed and atheroprotective regions, but it was nearly absent in the oscillatory shear stress (OSS)-exposed regions and lateral wall of arterial bifurcation. In cultured bovine aortic endothelial cells, PSS at mean shear stress (τ_{ave}) of 23 dyn/cm^2 upregulated Mn-SOD mRNA expression at a higher level than did OSS at τ_{ave} = 0.02 dyn/cm^2 ± 3.0 dyn·cm^{-2}·s^{-1} and at 1 Hz (PSS by 11.3 ± 0.4-fold vs. OSS by 5.0 ± 0.5-fold vs. static condition; $P < 0.05$, $n = 4$). By liquid chromatography and tandem mass spectrometry, it was found that PSS decreased the extent of low-density lipoprotein (LDL) nitration, whereas OSS increased nitration ($P < 0.05$, $n = 4$). In the presence of LDL, treatment with Mn-SOD small interfering RNA increased intracellular nitrotyrosine level ($P < 0.5$, $n = 4$), a fingerprint for nitrotyrosine formation. Our findings indicate that shear stress in the atheroprone versus atheroprotective regions regulates spatial variations in mitochondrial Mn-SOD expression with an implication for modulating LDL nitration.

superoxide dismutase; superoxide anion; nitric oxide; nitrotyrosine; low-density lipoprotein

ATHEROSCLEROTIC LESIONS PREFERENTIALLY develop in the lateral walls of vessel bifurcations and curvatures (34). Predilection sites for atherosclerosis are modulated by flow patterns to which the endothelium is exposed (13, 40). At the lateral wall of arterial bifurcations, a complex flow profile develops; flow separation and migrating stagnation points create oscillating shear stress (i.e., bidirectional with no net forward flow) (33). Oscillatory shear stress (OSS) increases oxidative stress, which promotes development of atherosclerotic plaque (14, 36, 46, 50, 52). In contrast, pulsatile flow downregulates adhesion molecules and reactive oxygen species in the medial wall of bifurcations or relatively straight segments.

Mitochondria are important sources of cellular superoxide anion ($O_2^{\cdot-}$) and H_2O_2 as a result of electron transport leak at complex I and III of the respiratory chain (17, 49). Mitochondrial superoxide dismutase (manganese SOD or Mn-SOD) is essential for life. Homozygous mice that are deficient in Mn-SOD die within days of birth (38). While expression of CuZn-SOD is regulated by blood flow (30, 44, 48, 51), it remains undefined if expression of Mn-SOD is influenced by specific shear stress patterns in the atheroprone versus atheroprotective regions.

Fluid shear stress influences the relative production of nitric oxide ($^{\cdot}NO$) and $O_2^{\cdot-}$ (10, 28, 37). In the atheroprotective regions, pulsatile shear stress (PSS) upregulates endothelial NO synthase (eNOS) gene expression (35) and eNOS phosphorylation mainly via the phosphatidylinositol 3-kinase (PI3K)-akt-mediated pathway (10, 18, 21, 22, 35) and downregulates vascular endothelial NADPH oxidases, a major source of $O_2^{\cdot-}$ (37). In the atheroprone regions, OSS downregulates eNOS activation and upregulates NADPH oxidase (11, 19, 22). OSS also attribute to the imbalance between $O_2^{\cdot-}$ and $^{\cdot}NO$ formation (27), favoring a diffusion-limited reaction to yield a potent oxidant, peroxynitrite ($O_2^{\cdot-}$ + $^{\cdot}NO$ → $ONOO^{-}$) (31, 47). Peroxynitrite reacts preferentially with tyrosine residues in proteins, leading to 3-nitrotyrosine, a fingerprint of $ONOO^{-}$ reactivity. In this context, we examined the spatial variations in Mn-SOD expression in medium-sized conductance blood vessels as a mechanism to influence $ONOO^{-}$ formation.

In the present study, the dynamic three-dimensional (3-D) computational fluid dynamics (CFD) model predicts PSS in atheroprotective versus OSS in atheroprone regions. Using explants of human coronary arterial bifurcations, we assessed whether PSS versus OSS influenced Mn-SOD immunohistolocalization. We demonstrated that Mn-SOD staining was prominent in the atheroprotective region, but it was nearly absent in the atheroprone regions. In cultured bovine aortic endothelial cells (BAEC), PSS upregulated Mn-SOD mRNA expression at a higher level than did OSS. PSS further modulated the extent of LDL protein nitration via Mn-SOD expression. Our findings indicate that the characteristics of shear stress influence spatial

---

variations in Mn-SOD expression with an implication for influencing LDL nitration.

METHODS

Three-Dimensional Bifurcation Model

The novel approach in the present study is to link specific shear stress patterns in the atheroprotective versus atheroprone regions of a 3-D bifurcation model with the corresponding Mn-SOD and nitrotyrosine localization from the explants of human coronary arteries. In addition, the molecular mechanisms by which specific shear stress patterns modulate endothelial Mn-SOD mRNA expression and LDL protein nitration were elucidated by cultured BAEC and/or human aortic endothelial cells (HAEC) in a 2-D dynamic flow system.

Generation of 3-D geometries and meshes. The construction of the bifurcation model and the associated flow patterns have been described previously (5, 20, 32). Briefly, the commercial CAD software, Pro Engineer Wildfire (version 3.0, Parametric Technology; Needham, MA), was used to construct the 3-D luminal geometrical model, which was then imported into a specialized preprocessing program for mesh generation (Gambit 2.3.16, Fluent; Lebanon, NH). The mesh consisted of tetrahedral elements and was imported into the main CFD solver (Fluent 6.2.16, Fluent) for flow simulation.

Blood flow model and boundary conditions. The 3-D Navier-Stokes equations were applied to solve the blood flow. The governing equations included mass and momentum equations, which were used to solve for laminar, incompressible, and non-Newtonian flow. The arterial wall was assumed to be rigid and impermeable. Characteristics such as inlet flow waveforms, blood viscosity, and vessel diameters were controlled to achieve the physiological conditions as previously reported in human left carotid artery (5, 20, 32). The pulsatile inlet flow rate was implemented by using 12 harmonics written in a user-defined C++ code.

Two-Dimensional Flow System

Two-dimensional dynamic flow channels were used to implement PSS and OSS obtained from the 3-D bifurcation model mentioned above. The 2-D flow system provides the precise and well-defined flow profiles across the width of the parallel flow chamber at various temporal variations in shear stress ($\delta\tau/\delta t$), frequency, and amplitude (26). BAEC were exposed to the characteristics of shear stress as obtained from the 3-D bifurcation model: *1*) PSS at a time-averaged shear stress (τ_{ave}) of 23 dyn/cm^2 with a temporal gradient ($\delta\tau/\delta t$) of 71 dyn·cm^{-2}·s^{-1}; and *2*) OSS at a τ_{ave} of 0.02 ± 3 dyn·cm^2 and $\delta\tau/\delta t$ of 0 dyn·cm^{-2}·s^{-1}. The 2-D model allowed for real-time monitoring of shear stress and quantitative real-time RT-PCR and Western blots from a sufficient number of vascular endothelial cells (EC) (24, 41, 42).

Endothelial Cell Culture

Confluent BAEC between *passages 4* and *7* were seeded on Cell-Tak cell adhesive and Collagen Type I (BD Bioscience, San Jose, CA) coated glass slides (5 cm^2) at 3×10^6 cells per slide. BAEC were grown to confluent monolayers in high glucose (4.5 g/l) DMEM supplemented with 10% heat-inactivated fetal bovine serum (Hyclone), 100 U/ml L-glutamine-penicillin-streptomycin (Sigma) for 48 h in 5% CO$_2$ at 37°C.

Immunohistochemistry of Human Coronary Arteries

Three human coronary arteries were obtained from explanted hearts of cardiac transplant patients. The protocol was approved by the Institutional Review Board of the University of Southern California, School of Medicine, and all volunteers gave informed consent. Cross sections of the left and right coronary arteries with and without atherosclerotic lesions were analyzed. Monoclonal antibodies were used for Mn-SOD (Upstate). Immunostaining was performed with standard techniques in frozen vascular tissue using biotinylated secondary antibodies and peroxidase staining. Diaminobenzidine was used as a chromogen, and the sections were counterstained with hematoxylin for visualization of intima, media, smooth muscle cells, and adventitia.

Counterstaining was performed to distinguish EC and smooth muscle cells in the media and/or intima proximal to the point of flow separation. EC and smooth muscle cells were stained with monoclonal antibodies specific for von Willebrand factor (vWF; 1:25 dilution) and β-actin (1:4,000 dilution) (Dakocytomation, Carpinteria, CA). Negative controls were performed by omitting the primary antibody. Positive controls included brain and kidney tissues.

Separation of LDL Subspecies by High-Performance Liquid Chromatography

Venous blood samples were obtained at the Atherosclerosis Research Unit from fasting adult human volunteers under institutional review board approval. Plasma was pooled and immediately separated by centrifugation at 1500 *g* for 10 min at 4°C. LDL (δ = 1.019 to 1.063 g/ml) was isolated from freshly separated plasma by preparative ultracentrifugation using a Beckman L8–55 ultracentrifuge and a SW-41 rotor. The technique used for separating LDL was similar to that described previously (45).

Endothelial Cell Exposure to Shear Stress

A dynamic flow system was used to implement temporal variations in shear stress ($\delta\tau/\delta t$); namely, PSS and OSS (24, 41, 42). Confluent BAEC were exposed to the flow conditions in the absence and presence of native LDL (50 µg/ml). After 4 h, BAEC were collected for quantitative real-time RT-PCR and Western blot analysis. In the presence of LDL, the culture medium was collected to measure apolipoprotein B (apoB)-100 nitration of the tyrosine residues.

Quantitative Real-Time RT-PCR

Confluent BAEC monolayers were exposed to PSS and OSS in a parallel plate flow system for 4 h as mentioned above. Total RNA was isolated using the RNeasy kit (Qiagen). RNA was reverse transcribed, followed by PCR amplification using the SuperScript III Platinum Two-Step qRT-PCR Kit with SYBR Green (Invitrogen, Carlsbad, CA). Oligonucleotides for Mn-SOD were *1*) forward primer 5′-GGA AGC CAT CAA ACG TGA CT-3′ and *2*) reverse primer 3′-AGC AGG GGG ATA AGA CCT GT-5′. Fidelity of the PCR reaction was determined by melting temperature analysis. For quantification of relative gene expression, the target sequence was normalized to 18s rRNA. The difference in cycle threshold values for various flow conditions vs. control was used to determine the relative difference in the levels of Mn-SOD mRNA expression.

LDL Protein Nitration

LDL suspended in medium was collected for analysis of protein nitration. Protein-bound nitrotyrosine formation in the recovered media was determined by stable isotope dilution liquid chromatography-tandem mass spectrometry (9) on a mass spectrometer (API 4000, Applied Biosystems, Foster City, CA) interfaced with an Aria LX Series HPLC multiplexing system (Cohesive Technologies, Franklin, MA). Synthetic $^{13}C_6$-labeled nitrotyrosine internal standard was added to samples for quantification of natural abundance of analytes. Simultaneously, a universal labeled precursor amino acid, $^{13}C_9,^{15}N_1$ tyrosine (for nitrotyrosine) was added to quantify the precursors and to assess potential intrapreparative artifactual oxidation during sample handling and analysis. Proteins were hydrolyzed under argon atmosphere in methane sulfonic acid,

and then samples passed over mini solid-phase C18 extraction columns (Supelclean LC-C18-SPE minicolumn, Supelco; Belle-fone, PA) before mass spectrometry analysis. Results were nor-malized to the content of the precursor amino acid, which was monitored within the same injection. Formation of $^{13}C_9$, ^{15}N-labeled nitrotyrosine was routinely monitored and negligible (i.e., <5% of the level of the natural abundance product observed).

Analysis for Nitrotyrosine

Confluent BAEC at fourth passage were pretreated with diethyldi-thiocarbamic acid (DIECA), a copper chelator to inhibit CuZn-SOD (1 mM for 60 min), and/or MnTMPyP, a Mn-SOD mimetic (10 μM for 30 min) in a serum-free DMEM medium. After DIECA and/or MnTMPyP were washed with PBS, BAEC were incubated with native LDL at 50 μg/ml for 4 h. LDL suspended in medium was collected to assess LDL protein nitration. LDL in the medium was concentrated by centrifugation at 3,000 rpm in Centriprep Centrifugal Filter Devices with YM-30 MW (Millipore). Dot blots were performed by spotting 15 μg of LDL. Membranes were soaked in methanol and washed with

Tris-buffered saline plus Tween (TBS-T). Samples were blocked in BSA and incubated with a polyclonal nitrotyrosine antibody overnight (1:3,000 dilution, Upstate), followed by incubation with horseradish peroxidase-conjugated goat anti-rabbit secondary antibody (1:10,000). Blots were detected using ECL chemiluminescence kit (Pierce, Rock-ford, IL). Positive control was established by treating LDL (0.2 mg/ml with peroxynitrite at 100 μM).

Silencing Mn-SOD mRNA in HAEC

Silencer small interfering (si)RNA was custom designed for Mn-SOD by Ambion (Austin, TX). The sense sequence was GGCCU-GAUUAUCUAAAAGCtt and the antisense sequence was GCU-UUUAGAUAAUCAGGCCtg. Confluent HAEC monolayers from *passages 4* to *9* were trypsinized and resuspended in standard growth medium to 100,000 cells/ml. siPORT NeoFX transfection reagent was diluted in OPTIMEM medium and incubated at room temperature for 10 min. Mn-SOD siRNA at a final concentration of 30 nM was diluted in OPTIMEM and mixed with diluted siPORT NeoFX reagent at room temperature for an additional 10 min. The transfection solution
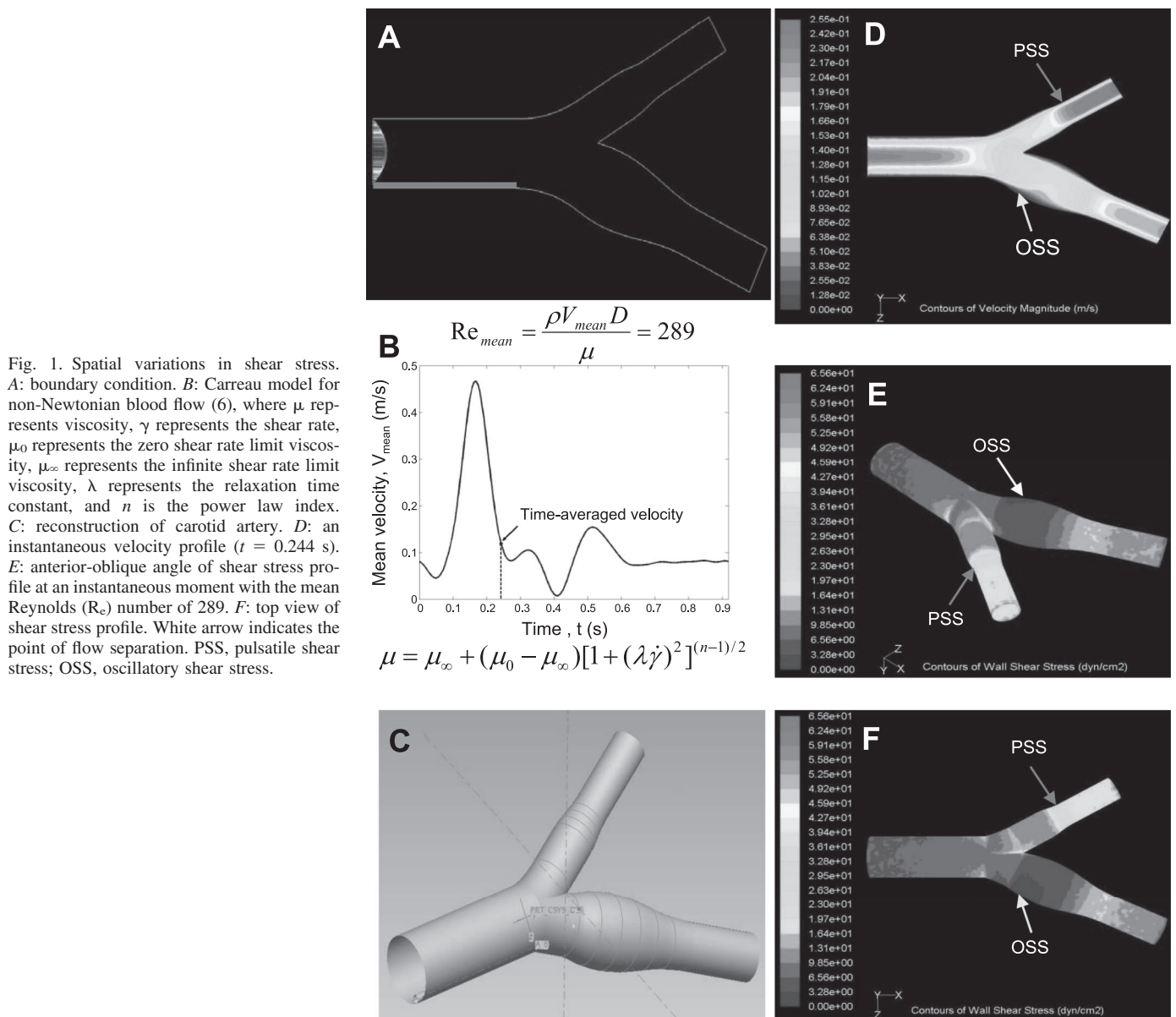
Fig. 1. Spatial variations in shear stress. *A*: boundary condition. *B*: Carreau model for non-Newtonian blood flow (6), where μ represents viscosity, γ represents the shear rate, μ_0 represents the zero shear rate limit viscosity, μ_∞ represents the infinite shear rate limit viscosity, λ represents the relaxation time constant, and *n* is the power law index. *C*: reconstruction of carotid artery. *D*: an instantaneous velocity profile ($t = 0.244$ s). *E*: anterior-oblique angle of shear stress profile at an instantaneous moment with the mean Reynolds (R_e) number of 289. *F*: top view of shear stress profile. White arrow indicates the point of flow separation. PSS, pulsatile shear stress; OSS, oscillatory shear stress.

$$\mathrm{Re}_{mean} = \frac{\rho V_{mean} D}{\mu} = 289$$

$$\mu = \mu_\infty + (\mu_0 - \mu_\infty)[1 + (\lambda \dot{\gamma})^2]^{(n-1)/2}$$

was dispensed into the six-well plates, followed by addition of HAEC in suspension. The medium was changed to standard growth medium after 24 h. The medium was replaced every other day until confluent HAEC monolayers developed. Quantitative RT-PCR and dot blot analysis were performed to validate effective silencing of Mn-SOD.

Western Analysis of Intracellular Nitrotyrosine Level

HAEC and siMn-SOD-treated HAEC were incubated with the CuZn-SOD chelator DIECA at 10 µM. The third HAEC sample was treated with the Mn-SOD mimetic MnTMPyP at 10 µM. After 1 h, the control sample (HAEC only) and the treated samples were incubated with LDL at 50 µg/ml. A blank sample was not treated with LDL or any other treatment. A positive control was treated with LDL, followed by $ONOO^-$ (100 µM). After 4 h, the cell lysates were collected. The Western analyses for nitrotyrosine were performed at a 1:3,000 dilution in TBS-T for primary monoclonal nitrotyrosine antibody (Upstate Cell Signaling Solutions) and 1:10,000 dilution for anti-mouse secondary antibody as previously described (27). Densitometry was performed using an NIH Scion Image Software (Scion, Frederick, MD).

Statistical Analysis

Data are expressed as means ± SD and were compared among separate experiments. For comparisons between two groups, two-sample independent-groups *t*-test was used. Comparisons of multiple values were made by one-way analysis of variance, and statistical significance among multiple groups was determined using the Tukey test (for pairwise comparisons of means between static-like and pulsatile flow conditions). *P* values < 0.05 were considered statistically significant.

RESULTS

Characteristics of Mean Shear Stress in a 3-D Bifurcation Model

The intention of our 3-D model was to link specific shear stress profiles with spatial variations in Mn-SOD expression. We proposed that Mn-SOD expression influenced nitrotyrosine formation. By using non-Newtonian blood flow, the dynamic 3-D CFD code demonstrated shear stress at the lateral versus medial wall of internal and external carotid arteries, and the divider of the bifurcation (6) (Fig. 1, *A–C*). At a given instantaneous moment ($t = 0.244$ s), magnitude of shear stress was the highest at the divider of bifurcation and lowest at the point of flow separation. For a Reynolds number of 289 (representative of human carotid blood flow), the time-averaged shear stress of pulsatile flow along the medial wall of internal carotid artery ranged from 20 to 26 dyn/cm^2 (Fig. 1, *E* and *F*), and the point of flow separation oscillated between −3 and 3 dyn/cm^2 in response to cardiac contraction. The shear stress valves
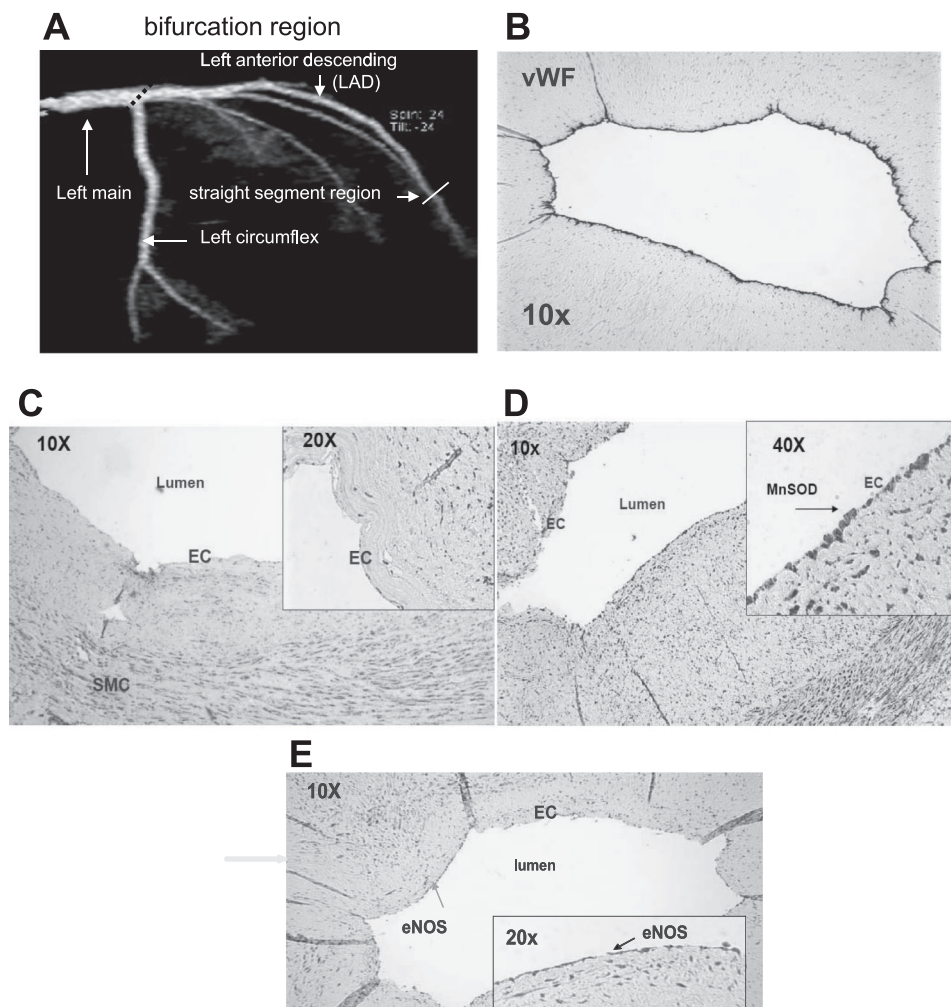
Fig. 2. Mn-SOD immunostaining of a section of left coronary artery. *A*: a representative left coronary artery and its branches. *B*: von Willebrand Factor (vWF) staining for endothelial cells (EC). *C*: at the left main bifurcation (OSS-exposed region), Mn-SOD staining was absent in the luminal EC. *D*: in straight segment of left anterior descending (LAD) artery (PSS-exposed region), Mn-SOD staining was prevalent throughout the entire luminal EC. *E*: endothelial nitric oxide (NO) synthase (eNOS) staining was positive. This section was previously reported to be eNOS positive (27). SMC, smooth muscle cells.

derived from the 3-D CFD code provided a basis to assess spatial variations in Mn-SOD expression.

Spatial Variations in Mn-SOD and Nitrotyrosine Immunostaining

In the present study, Mn-SOD staining was absent in the OSS-exposed regions, but it was prominent throughout the entire endothelium in the PSS-exposed regions (Fig. 2). vWF staining and eNOS staining was positive in the entire luminal EC in the PSS-exposed region (27). In contrast, nitrotyrosine staining was prominent in the arterial bifurcation regions where eNOS and Mn-SOD staining were nearly absent (Fig. 3). The integration of CFD and immunohisto-localizations suggests that spatial variation in Mn-SOD expression was influenced by specific shear stress patterns. We have recently reported that nitrotyrosine immunohistostaining was prominent in the OSS-exposed regions but absent in the PSS-exposed regions (27). Our present study
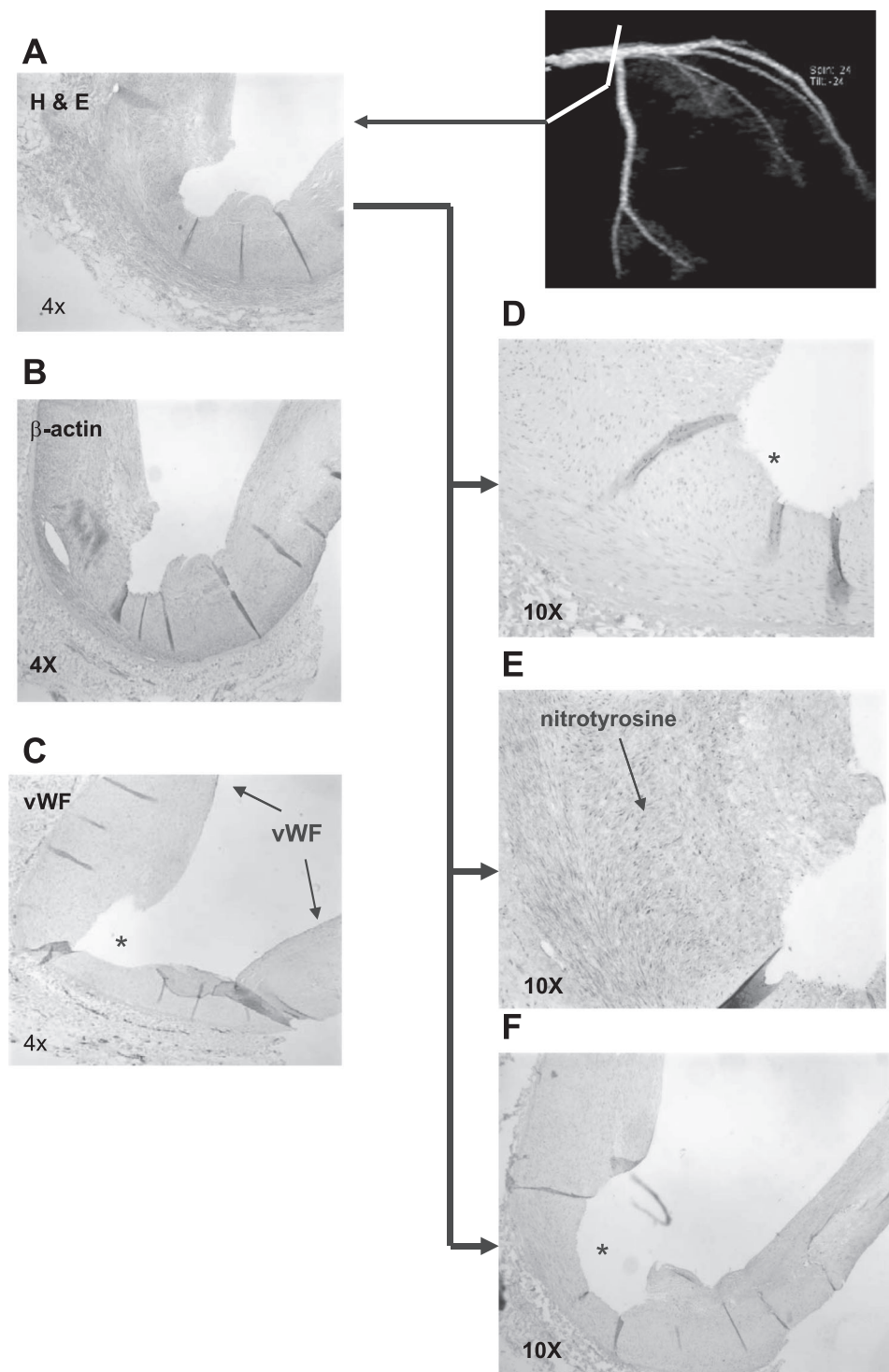
Fig. 3. Nitrotyrosine immunostaining of left main coronary arterial bifurcation. *A*: counterstaining with hematoxylin and eosin (H & E). *B*: β-actin for SMC. *C*: vWF for EC. *D*: MnSOD staining was absent in the luminal endothelium. *E*: nitrotyrosine staining was prevalent in the SMC. *F*: eNOS staining was absent. *Lumen that was denuded in EC (*C*, *D*, and *F*).

supported the notion that Mn-SOD staining was prominent in the PSS-exposed regions where nitrotyrosine was nearly absent, but Mn-SOD was absent in the OSS-exposed regions where nitrotyrosine was prominent.

Flow Regulation of Mn-SOD mRNA Expression and Nitrotyrosine Formation

BAEC were exposed to shear stress in a dynamic flow system simulating flow profiles in the PSS- and OSS-exposed regions of a 3-D arterial bifurcation. Endothelial Mn-SOD mRNA was significantly upregulated in response to shear stress. Specifically, PSS induced an 11.3-fold increase, whereas OSS induced a 5-fold increase (Fig. 4B). Western blot analyses corroborated Mn-SOD protein expression (Fig. 4D). CuZn-SOD mRNA expression was increased by 2.3-fold in response

to PSS (Fig. 4A). EC-SOD that was expressed in smooth muscle cells was unresponsive to shear stress (Fig. 4C). To test the pathophysiological significance of Mn-SOD expression, we assessed LDL particles as a surrogate marker for protein nitration by $ONOO^-$ (27). The LDL apoB-100 residues were analyzed by liquid chromatography/electro spray ionization/tandem mass spectrometry (LC/ESI/MS/MS). OSS increased the level of protein nitration, whereas PSS significantly decreased the level in comparison with the control under static conditions (Fig. 5).

The Effects of Mn-SOD siRNA on Extra- and Intracellular Nitrotyrosine Levels

To test the role of Mn-SOD on LDL nitration, we treated HAEC with Mn-SOD siRNA (siMn-SOD), followed by incuba-
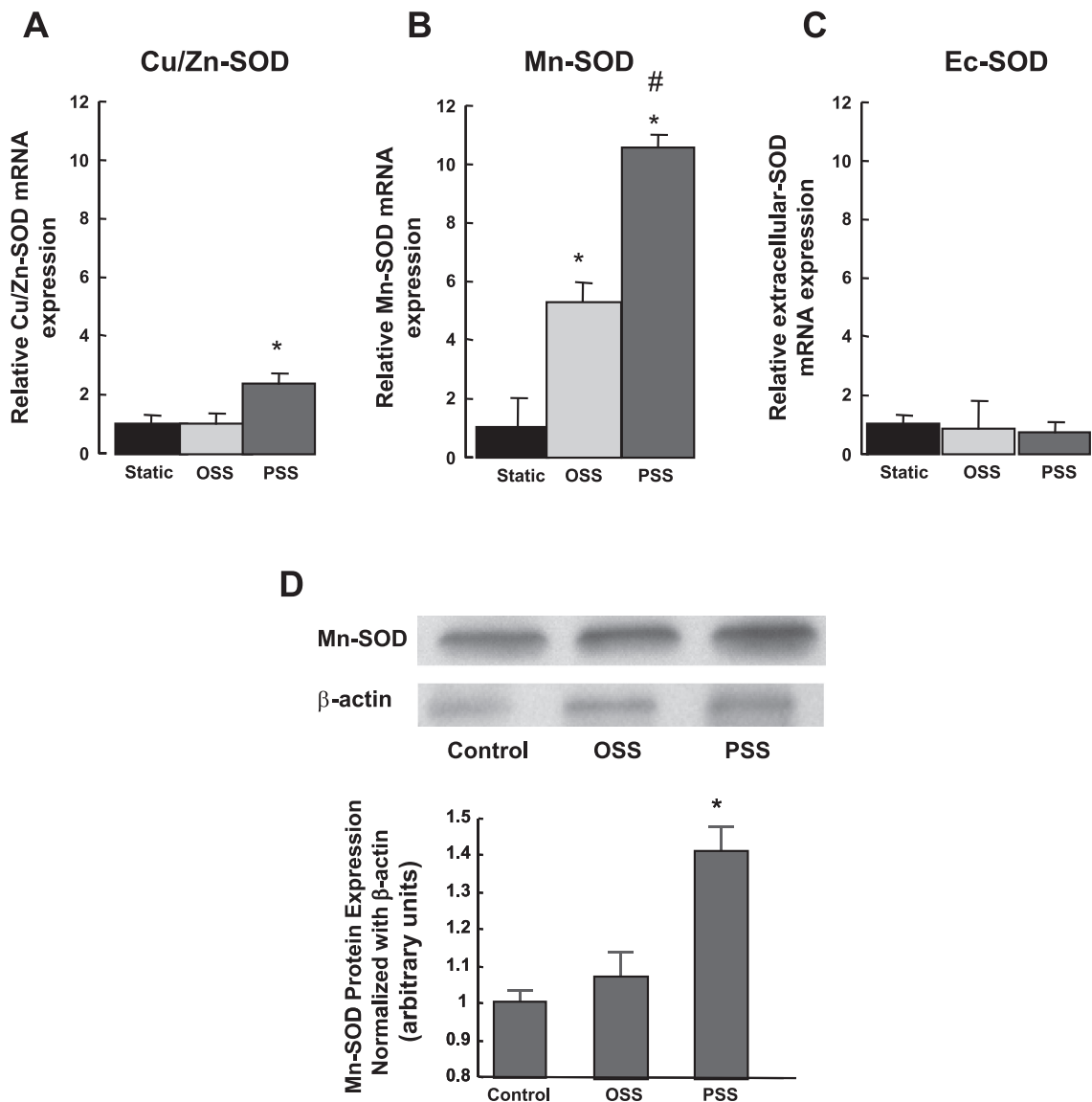
Fig. 4. SOD isoform expression in bovine aorta endothelial cells (BAEC) in response to OSS and PSS. Cu/Zn-, Mn-, and extracellular-SOD mRNA expression was normalized to 18s RNA (*$P < 0.05$ in comparison to the static samples; $n = 3$). A: Cu/Zn-SOD expression was upregulated by 2.3-fold in response to PSS. B: Mn-SOD mRNA expression was upregulated by 5-fold in response to OSS and by 11.4-fold to PSS (*$P < 0.05$ vs. static, #$P < 0.05$ vs. OSS, $n = 3$). C: EC-SOD remained relatively unresponsive to shear stress. D: Mn-SOD protein expression. The increase in Mn-SOD expression was not statistically significant in response to OSS. PSS upregulated Mn-SOD expression by 1.4-fold (*$P < 0.05$, $n = 4$).
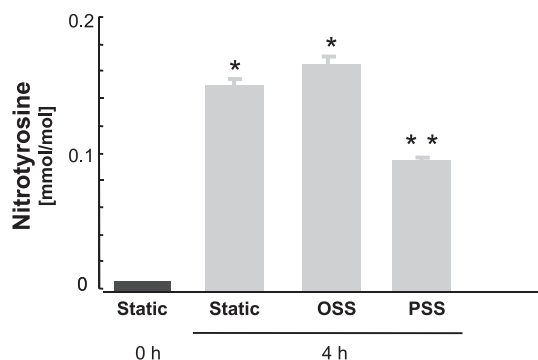
Fig. 5. Liquid chromatography/electron spray ionization/mass spectroscopy/ mass spectroscopy analyses of LDL protein nitration as a fingerprint of nitrotyrosine formation. LDL nitration occurred when BAEC were treated with native LDL at 4 h. OSS further increased the level of LDL nitration, whereas PSS decreased the level at 4 h (*$P < 0.05$ vs. static at 0 h, **$P < 0.05$ vs. OSS; $n = 4$).

tion with native LDL. Dot blot analysis was performed to assess extracellular LDL nitration. In the presence of MnTMPyP, a Mn-SOD mimetic, the level of nitrotyrosine or LDL nitration was reduced. (Fig. 6). In siMn-SOD-treated HAEC, the level was significantly higher than that of MnTMPyP-treated HAEC. Western analysis was performed to assess intracellular nitrotyrosine levels in siMn-SOD-treated HAEC (Fig. 7). Mn-SOD siRNA significantly increased intracellular nitrotyrosine level compared with the native LDL-treated BAEC. Our observation corroborated the notion that Mn-SOD expression influenced the extent of LDL protein nitration and that PSS attenuated the extent of LDL nitration via Mn-SOD upregulation. The CFD
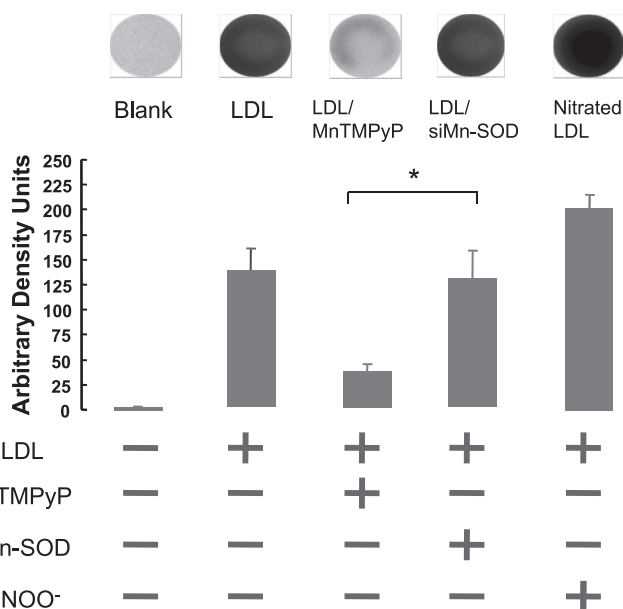
Fig. 6. Dot blot analysis of extracellular nitrotyrosine levels in the presence of native LDL. Blank refers to samples without LDL treatment. Native LDL induced an increase in LDL nitrotyrosine level. Addition of Mn-SOD mimetic (MnTMPyP) significantly attenuated the nitrotyrosine level. Positive control indicates samples treated with ONOO⁻. The nitrotyrosine level in small interfering (si)Mn-SOD-treated human aorta endothelial cells (HAEC) was significantly higher than in MnTMPyP-treated HAEC. The differences between siMn-SOD plus LDL-treated samples and LDL-treated samples were statistically insignificant (*$P > 0.05$, $n = 4$).
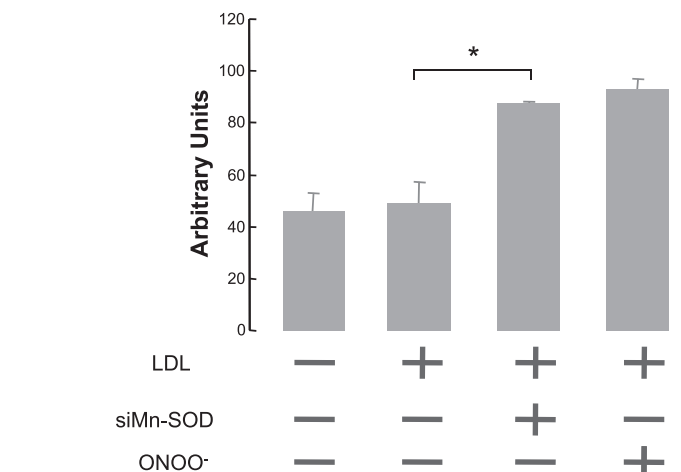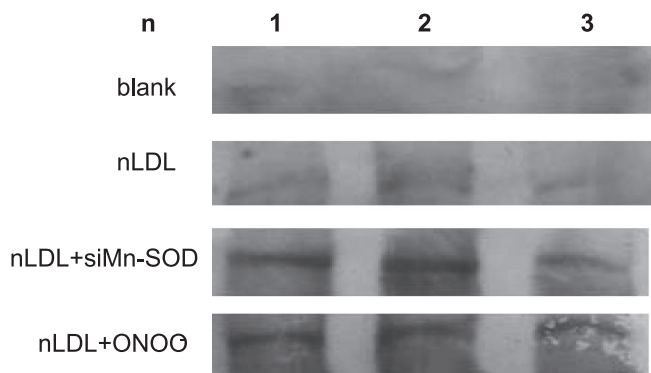
Fig. 7. Western analysis of intracellular nitrotyrosine levels in native LDL (nLDL)-treated BAEC. Silencing Mn-SOD significantly increased nitrotyrosine level. Blank refers to samples without LDL treatment. Positive control indicates samples treated with ONOO⁻ (*$P < 0.05$, $n = 3$).

code enabled us to link specific shear stress profiles with spatial variations in Mn-SOD expression with an implication for arterial nitrotyrosine formation.

DISCUSSION

In the present study, we demonstrated that shear stress influenced spatial variations in Mn-SOD expression. That OSS and PSS patterns may contribute to this phenomenon is supported by four lines of evidence: *1*) the 3-D computational fluid dynamic model predicts regions of OSS and PSS in the arterial bifurcations; *2*) immunohistolocalization and physiological study showed that Mn-SOD staining was prominent in the PSS-exposed regions but was absent in OSS-exposed regions; *3*) nitrotyrosine staining was absent in the PSS-exposed regions but was present in the OSS-exposed regions; and *4*) PSS and OSS differentially regulated LDL protein nitration via Mn-SOD mRNA expression in cultured EC.

The 3-D CFD code confirmed that the EC in medial wall or the straight segment of vessels experience PSS, whereas EC near the point of flow separation experience OSS in the atherosclerosis-prone regions (34). The mean shear stress values obtained from the 3-D model were implemented in the 2-D flow system to elucidate SOD isoform mRNA expression and LDL protein nitration. Blackman et al. (7) reported a cone-and-plate system that was capable of generating precise athero-

protective versus atherogenic waveforms from human carotid arteries. Compared with the cone-and-plate system, our 2-D microfluidic channel was designed to uniformly generate specific pulsatile versus oscillatory shear stress at various slow rates (24).

Mn-SOD is an important dismutase of reactive oxygen species acting in the mitochondria matrix. Oxidative phosphorylation in mitochondria ATP occurs as electrons are transferred from NADH or $FADH_2$ to molecular oxygen. The transfer of >98% of electrons by the electron transport chain is coupled with the production of ATP, and 1.5% to 2% of electrons leak out to form $O_2^{\cdot-}$, which is dismutased by Mn-SOD (39). In response to pathological conditions such as reperfusion injury, the electron transport chain may become uncoupled, leading to an increase in $O_2^{\cdot-}$ production (8). Bernal-Mizrachi et al. (4) reported respiratory uncoupling in smooth muscle cells caused atherosclerosis in mice. In apoE-deficient mice (apoE$^{-/-}$) (3), the normally expressed levels of Mn-SOD protect against oxidative stress and endothelial dysfunction.

We compared the OSS-exposed regions, such as bifurcations or greater curvatures, with the PSS-exposed regions, such as the relative straight segments or medial wall of arterial bifurcations. Our finding supports the notion that spatial variations in shear stress influence MnSOD staining in three out of three explants of human coronary arteries from patients diagnosed with ischemic cardiomyopathy. The immunohistochemistry analysis in Fig. 2 was representative of a section of left anterior distal arteries where PSS occurred and atherosclerotic lesions were absent; and Fig. 3 was representative of lateral wall of an arterial bifurcation where OSS developed and atherosclerotic lesions were present. We previously reported that nitrotyrosine staining was prominent in the OSS-exposed region but was absent in the PSS-exposed regions (27). In PSS-exposed regions, Mn-SOD staining was prominent but nitrotyrosine staining was absent, and Mn-SOD expression influenced the extent of LDL nitration (Figs. 5 and 6).

Our data also suggest that Mn-SOD and CuZn-SOD, but not EC-SOD, are responsive to shear stress in vascular EC. EC-SOD is synthesized in smooth muscle cells, and CuZn-SOD is prevalent in vascular EC. Inoue et al. (30) reported that CuZn-SOD in HAEC is upregulated in response to laminar flow. Despite different experimental designs, namely, *1*) the cell type (BAEC versus HAEC), *2*) duration of flow exposure (4 vs. 24 h), *3*) magnitude and characteristic of shear stress profiles, and *4*) flow models (cone-and-plate vs. pulsatile parallel plate), our finding in CuZn-SOD expression in response to PSS is in agreement with that of Inoue et al. (30). Moreover, we demonstrated that shear stress regulated Mn-SOD and CuZn-SOD expression in both BAEC and HAEC. Whether there exists a shear stress-responsive element in Mn-SOD gene remains undefined; however, a redox-sensitive mechanism was implicated in Mn-SOD promoter activity via a negative PI3K-akt-forkhead pathway and a positive PKC-NF-κB pathway (1).

Several studies have examined effects of SOD isoforms on endothelial function and atherogenesis. EC-SOD plays a significant protective role on arterial pressure, vascular function, or vascular levels of oxidative stress in spontaneous hypertensive rats (12). Similarly, cytosolic CuZn-SOD is atheroprotective, playing a critical role in limiting angiotensin II-induced endothelial cell dysfunction (15). The CuZn-SOD-deficient (CuZn-SOD$^{-/-}$) mice showed an increased superoxide level

and altered vascular responsiveness compared with the wild-type littermates (16). The protein-encoded Mn-SOD transmigrate to mitochondria. Mn-SOD-deficient mice (Mn-SOD$^{-/-}$) were reported to develop more atherosclerosis (3). However, the relative contribution of CuZn-SOD and Mn-SOD to dismutate superoxide anion in response to shear stress requires further investigations.

Pulsatile flow significantly reduced the ratios of oxidatively modified forms of LDL relative to static conditions, whereas oscillating flow increased LDL oxidation (28), leading to upregulation of adhesion molecules and recruitment of monocytes (23, 25). In the present study, OSS increased the level of tyrosine nitration and oxidation products in LDL, whereas PSS decreased the levels of both tyrosine nitration and oxidation. Nitration of tyrosine residues by $ONOO^-$ resulted in a more hydrophilic residue, thus altering the structure of α-helices of apoB-100 of the LDL particles (2, 29).

We analyzed LDL protein nitration at both protein and amino acid levels. The former was established by dot blot analysis. Using anti-nitrotyrosine antibody, we suspended LDL in medium to assess LDL protein nitration. The latter was performed by LC/ESI/MS/MS. The proteomic approach allowed for identification of the specific apoB-100 tyrosine residue nitration in α- and β-helices as follows: α-1 (Tyr^{144}), α-2 (Tyr^{2524}), β-2 (Tyr^{3295}), α-3 (Tyr^{4116}), and β-2 (Tyr^{4211}) (27). Both lipid peroxidation and protein nitration account for apoB-100 protein unfolding and consequential increase in modified LDL binding and uptake by endothelial cells.

Antioxidant gene expression is present in mouse aortic arch where disturbed flow, including OSS, develops. Passerini et al. (43) reported a host of antioxidant gene expression from adult porcine aortic arch by genomics. The authors suggested that there is an evolutionary benefit to favor a moderate level of atheroprotective gene expression in the atheroprone regions such as curvatures and bifurcations. In this context, our in vitro findings between OSS and PSS complement those of mouse genomic analysis.

In summary, our bifurcation model predicts the characteristics of shear stress in the PSS- and OSS-exposed regions of the arterial bifurcation. Explants of human coronary arteries enabled us to assess the pathophysiological significance of this model in terms of Mn-SOD immunohistolocalization. Our findings strongly support the notion that pulsatile and oscillatory shear stress modulated spatial variations in Mn-SOD expression and that Mn-SOD plays an important role in nitrotyrosine formation.

REFERENCES

1. **Abid MR, Schoots IG, Spokes KC, Wu SQ, Mawhinney C, Aird WC.** Vascular endothelial growth factor-mediated induction of manganese superoxide dismutase occurs through redox-dependent regulation of forkhead and I kappa B/NF-kappa B. *J Biol Chem* 279: 44030–44038, 2004.

2. **Asatryan L, Hamilton R, Mario Isas J, Hwang J, Kayed R, Sevanian A.** LDL phospholipid hydrolysis produces modified electronegative particles with an unfolded apoB-100 protein. *J Lipid Res* 46: 115–122, 2005.

3. **Azumi H, Inoue N, Ohashi Y, Terashima M, Mori T, Fujita H, Awano K, Kobayashi K, Maeda K, Hata K, Shinke T, Kobayashi S, Hirata K, Kawashima S, Itabe H, Hayashi Y, Imajoh-Ohmi S, Itoh H, MY.** Superoxide generation in directional coronary atherectomy specimens of patients with angina pectoris: important role of NAD(P)H oxidase. *Arterioscler Thromb Vasc Biol* 22: 1838–1844, 2002.

4. **Bernal-Mizrachi C, Gates AC, Weng S, Imamura T, Knutsen RH, DeSantis P, Coleman T, Townsend RR, Muglia LJ, Semenkovich CF.** Vascular respiratory uncoupling increases blood pressure and atherosclerosis. *Nature* 435: 502–506, 2005.

5. **Bharadvaj BK, Mabon RF, Giddens DP.** Steady flow in a model of the human carotid bifurcation. 1. Flow visualization. *J Biomech* 15: 349–362, 1982.

6. **Bird RB, Armstrong RC, Hassager O.** *Dynamics of Polymeric Liquids. Fluid Mechanics*, New York: Wiley, 1977, vol. 1.

7. **Blackman BR, Garcia-Cardena G, Gimbrone MA.** A new in vitro model to evaluate differential responses of endothelial cells to simulated arterial shear stress waveforms. *J Biomech Eng* 124: 397–407, 2002.

8. **Boveris A, Cadenas E, Stoppani AO.** Role of ubiquinone in the mitochondrial generation of hydrogen peroxide. *Biochem J* 156: 435–444, 1976.

9. **Brennan ML, Wu W, Fu X, Shen Z, Song W, Frost H, Vadseth C, Narine L, Lenkiewicz E, Borchers MT, Lusis AJ, Lee JJ, Lee NA, Abu-Soud HM, Ischiropoulos H, Hazen SL.** A tale of two controversies: defining both the role of peroxidases in nitrotyrosine formation in vivo using eosinophil peroxidase and myeloperoxidase-deficient mice, and the nature of peroxidase-generated reactive nitrogen species. *J Biol Chem* 277: 17415–17427, 2002.

10. **Chatzizisis YS, Coskun AU, Jonas M, Edelman ER, Feldman CL, Stone PH.** Role of endothelial shear stress in the natural history of coronary atherosclerosis and vascular remodeling: molecular, cellular, and vascular behavior. *J Am Coll Cardiol* 49: 2379–2393, 2007.

11. **Cheng C, van Haperen R, de Waard M, van Damme LCA, Tempel D, Hanemaaijer L, van Cappellen GWA, Bos J, Slager CJ, Duncker DJ, van der Steen AFW, de Crom R, Krams R.** Shear stress affects the intracellular distribution of eNOS: direct demonstration by a novel in vivo technique. *Blood* 106: 3691–3698, 2005.

12. **Chu Y, Alwahdani A, Iida S, Lund DD, Faraci FM, Heistad DD.** Vascular effects of the human extracellular superoxide dismutase R213G variant. *Circulation* 112: 1047–1053, 2005.

13. **Davies PF, Dewey CF Jr, Bussolari SR, Gordon EJ, Gimbrone MA Jr.** Influence of hemodynamic forces on vascular endothelial function. In vitro studies of shear stress and pinocytosis in bovine aortic cells. *J Clin Invest* 73: 1121–1129, 1984.

14. **De Keulenaer GW, Chappell DC, Ishizaka N, Nerem RM, Alexander RW, Griendling KK.** Oscillatory and steady laminar shear stress differentially affect human endothelial redox state: role of a superoxide-producing NADH oxidase. *Circ Res* 82: 1094–1101, 1998.

15. **Didion SP, Kinzenbaw DA, Faraci FM.** Critical role for CuZn-superoxide dismutase in preventing angiotensin II-induced endothelial dysfunction. *Hypertension* 46: 1147–1153, 2005.

16. **Didion SP, Ryan MJ, Didion LA, Fegan PE, Sigmund CD, Faraci FM.** Increased superoxide and vascular dysfunction in CuZnSOD-deficient mice. *Circ Res* 91: 938–944, 2002.

17. **Esposito LA, Melov S, Panov A, Cottrell BA, Wallace DC.** Mitochondrial disease in mouse results in increased oxidative stress. *Proc Natl Acad Sci USA* 96: 4820–4825, 1999.

18. **Fleming I, Fisslthaler B, Dixit M, Busse R.** Role of PECAM-1 in the shear-stress-induced activation of Akt and the endothelial nitric oxide synthase (eNOS) in endothelial cells. *J Cell Sci* 118: 4103–4111, 2005.

19. **Gambillara V, Chambaz C, Montorzi G, Roy S, Stergiopulos N, Silacci P.** Plaque-prone hemodynamics impair endothelial function in pig carotid arteries. *Am J Physiol Heart Circ Physiol* 290: H2320–H2328, 2006.

20. **Gijsen FJH, van de Vosse FN, Janssen JD.** The influence of the non-Newtonian properties of blood on the flow in large arteries: steady flow in a carotid bifurcation model. *J Biomech* 32: 601–608, 1999.

21. **Go YM, Boo YC, Park H, Maland MC, Patel R, Pritchard KA, Fujio Y, Walsh K, Darley-Usmar V, Jo H.** Protein kinase B/Akt activates c-Jun NH$_2$-terminal kinase by increasing NO production in response to shear stress. *J Appl Physiol* 91: 1574–1581, 2001.

22. **Harrison DG, Widder J, Grumbach I, Chen W, Weber M, Searles C.** Endothelial mechanotransduction, nitric oxide and vascular inflammation. *J Int Med Res* 259: 351–363, 2006.

23. **Honda HM, Hsiai T, Wortham CM, Chen MD, Lin H, Navab M, Demer LL.** A complex flow pattern of low shear stress and flow reversal promotes monocyte binding to endothelial cells. *Atherosclerosis* 158: 385–390, 2001.

24. **Hsiai TK, Cho SK, Honda HM, Hama S, Navab M, Demer LL, Ho CM.** Endothelial cell dynamics under pulsating flows: significance of high versus low shear stress slew rates (delta tau/delta t). *Ann Biomed Eng* 30: 646–656, 2002.

25. **Hsiai TK, Cho SK, Wong PK, Ing M, Salazar A, Sevanian A, Navab M, Demer LL, Ho CM.** Monocyte recruitment to endothelial cells in response to oscillatory shear stress. *FASEB J* 17: 1648–1657, 2003.

26. **Hsiai TK, Cho SK, Wong PK, Ing MH, Salazar A, Hama S, Navab M, Demer LL, Chih-Ming H.** Micro sensors: linking real-time oscillatory shear stress with vascular inflammatory responses. *Ann Biomed Eng* 32: 189–201, 2004.

27. **Hsiai TK, Hwang J, Barr ML, Correa A, Hamilton R, Alavi M, Rouhanizadeh M, Cadenas E, Hazen SL.** Hemodynamics influences vascular peroxynitrite formation: implication for low-density lipoprotein apo-B-100 nitration. *Free Radic Biol Med* 42: 519–529, 2007.

28. **Hwang J, Ing MH, Salazar A, Lassegue B, Griendling K, Navab M, Sevanian A, Hsiai TK.** Pulsatile versus oscillatory shear stress regulates NADPH oxidase subunit expression: implication for native LDL oxidation. *Circ Res* 93: 1225–1232, 2003.

29. **Hwang J, Rouhanizadeh M, Hamilton RT, Lin TC, Eiserich JP, Hodis HN, Hsiai TK.** 17 beta-Estradiol reverses shear-stress-mediated low density lipoprotein modifications. *Free Radic Biol Med* 41: 568–578, 2006.

30. **Inoue N, Ramasamy S, Fukai T, Nerem RM, Harrison DG.** Shear stress modulates expression of Cu/Zn superoxide dismutase in human aortic endothelial cells. *Circ Res* 79: 32–37, 1996.

31. **Irani K.** Oxidant signaling in vascular cell growth, death, and survival: a review of the roles of reactive oxygen species in smooth muscle and endothelial cell mitogenic and apoptotic signaling. *Circ Res* 87: 179–183, 2000.

32. **Kim CSS, Kiris C, Kwak D, David T.** Numerical simulation of local blood flow in the carotid and cerebral arteries under altered gravity. *J Biomech Eng* 128: 194–202, 2006.

33. **Ku DN.** Blood flow in arteries. *Annu Rev Fluid Mech* 29: 399–434, 1997.

34. **Ku DN, Giddens DP, Zarins CK, Glagov S.** Pulsatile flow and atherosclerosis in the human carotid bifurcation. Positive correlation between plaque location and low and oscillating shear-stress. *Arteriosclerosis* 5: 293–302, 1985.

35. **Lam CF, Peterson TE, Richardson DM, Croatt AJ, d'Uscio LV, Nath KA, Katusic ZS.** Increased blood flow causes coordinated upregulation of arterial eNOS and biosynthesis of tetrahydrobiopterin. *Am J Physiol Heart Circ Physiol* 290: H786–H793, 2006.

36. **Landmesser U, Harrison DG.** Oxidant stress as a marker for cardiovascular events. Ox marks the spot. *Circulation* 104: 2638–2640, 2001.

37. **Li Y, Zheng J, Bird IM, Magness RR.** Effects of pulsatile shear stress on signaling mechanisms controlling nitric oxide production, endothelial nitric oxide synthase phosphorylation, and expression in ovine fetoplacental artery endothelial cells. *Endothelium* 12: 21–39, 2005.

38. **Li YB, Huang TT, Carlson EJ, Melov S, Ursell PC, Olson TL, Noble LJ, Yoshimura MP, Berger C, Chan PH, Wallace DC, Epstein CJ.** Dilated cardiomyopathy and neonatal lethality in mutant mice lacking manganese superoxide-dismutase. *Nat Genet* 11: 376–381, 1995.

39. **Madamanchi NR, Vendrov A, Runge MS.** Oxidative stress and vascular disease. *Arterioscler Thromb Vasc Biol* 25: 29–38, 2005.

40. **Malek AM, Alper SL, Izumo S.** Hemodynamic shear stress and its role in atherosclerosis. *JAMA* 282: 2035–2042, 1999.

41. **Nerem RM, Alexander RW, Chappell DC, Medford RM, Varner SE, Taylor WR.** The study of the influence of flow on vascular endothelial biology. *Am J Med Sci* 316: 169–175, 1998.

42. **Papadaki M, McItire LV.** Quantitative measurement of shear-stress effects on endothelial cells. In: *Methods in Molecular Medicine. Tissue Engineering Methods and Protocols*, edited by Morgan JR, Yarmush ML. Totowa, NJ: Humana, 1998, vol. 18, p. 577–593.

43. **Passerini AG, Polacek DC, Shi C, Francesco NM, Manduchi E, Grant GR, Pritchard WF, Powell S, Chang GY, Stoeckert CJ Jr, Davies PF.** Coexisting proinflammatory and antioxidative endothelial transcription profiles in a disturbed flow region of the adult porcine aorta. *Proc Natl Acad Sci USA* 101: 2482–2487, 2004.

44. **Rush JWE, Laughlin MH, Woodman CR, Price EM.** SOD-1 expression in pig coronary arterioles is increased by exercise training. *Am J Physiol Heart Circ Physiol* 279: H2068–H2076, 2000.

45. **Sevanian A, Seraglia R, Traldi P, Rossato P, Ursini F, HNH.** Analytical approaches to the measurement of plasma cholesterol oxidation products using gas- and high-performance liquid chromatography/mass spectrometry. *Free Radic Biol Med* 17: 397–410, 1994.

46. **Sorescu D, Weiss D, Lassegue B, Clempus RE, Szocs K, Sorescu GP, Valppu L, Quinn MT, Lambeth JD, Vega JD, Taylor WR, Griendling KK.** Superoxide production and expression of nox family proteins in human atherosclerosis. *Circulation* 105: 1429–1435, 2002.

47. **Sowers JR, Epstein M, Frohlich ED.** Diabetes, hypertension, and cardiovascular disease: an update. *Hypertension* 37: 1053–1059, 2001.

48. **Tao J, Yang Z, Wang JM, Wang LC, Luo CF, Tang AL, Dong YG, Ma H.** Shear stress increases Cu/Zn SOD activity and mRNA expression in human endothelial progenitor cells. *J Hum Hypertens* 21: 353–358, 2007.

49. **Wallace DC.** Mitochondrial genetics: a paradigm for aging and degenerative diseases? *Science* 256: 628–632, 1992.

50. **Witztum JR.** The oxidation hypothesis of atherosclerosis. *Lancet* 344: 793–795, 1994.

51. **Woodman CR, Muller JM, Rush JWE, Laughlin MH, Price EM.** Flow regulation of ecNOS and Cu/Zn SOD mRNA expression in porcine coronary arterioles. *Am J Physiol Heart Circ Physiol* 276: H1058–H1063, 1999.

52. **Ziegler T, Bouzourene K, Harrison VJ, Brunner HR, Hayoz D.** Influence of oscillatory and unidirectional flow environments on the expression of endothelin and nitric oxide synthase in cultured endothelial cells. *Arterioscler Thromb Vasc Biol* 18: 686–692, 1998.